Applied Catalysis B: Environmental 111–112 (2012) 515–526

Contents lists available at SciVerse ScienceDirect

Applied Catalysis B: Environmental

journal homepage: www.elsevier.com/locate/apcatb

Oxygen reduction reaction (ORR) activity and durability of carbon supported PtM (Co, Ni, Cu) alloys: Influence of particle size and non-noble metals

Kaushik Jayasayee [1], J.A. Rob Van Veen, Thirugnasambandam G. Manivasagam, Serdar Celebi, Emiel J.M. Hensen, Frank A. de Bruijn *

Schuit Institute of Catalysis, Eindhoven University of Technology, 5600 MB, The Netherlands

ARTICLE INFO

Article history:
Received 10 July 2011
Received in revised form 27 October 2011
Accepted 1 November 2011
Available online 7 November 2011

Keywords:
Pt alloys
ORR activity
PEMFC
Fuel cells
Durability

ABSTRACT

Carbon supported platinum and platinum alloys (PtCo, PtNi and PtCu) for PEMFC cathodes were prepared and studied for their oxygen reduction reaction activity and durability under potential cycling at 80 °C in 0.5 M $HClO_4$. Catalysts with different metal alloy composition and particle size were synthesized by annealing at different temperatures to discriminate between the effects of alloying and particle size on the electrocatalytic activity and durability. XRD was used for the structural characterization of pristine catalysts, while the bulk compositions were analyzed by EDS before and after durability tests. XPS was employed to determine the surface composition of selected alloys after durability tests. The particle size of the fresh and aged catalysts was determined by TEM. Rapid dealloying, particularly from non-noble metal rich alloys, was already witnessed for the alloys potentially cycled at room temperature. Significant particle growth depending on the initial particle size was observed for both Pt and Pt alloys after the durability tests. For the alloys with similar initial particle size, the initial electrocatalytic activity depends on the initial alloy composition. Although a 3-fold enhancement in the ORR activity was observed for the non-noble metal rich alloys after initial dealloying, the specific activity of Pt and Pt alloys becomes quite similar at the end of the durability tests. Annealing of Pt/C and Pt alloys at 950 °C results in catalysts with the highest specific and mass activity and with the highest stability.

1. Introduction

Large scale commercialization of polymer electrolyte membrane fuel cell (PEMFC) systems can only take off when further cost reduction and durability improvements are realized [1,2]. Platinum supported on carbon is generally used as the catalyst for the anode (hydrogen oxidation) and cathode (oxygen reduction) reactions. Despite being the most active element for the oxygen reduction reaction (ORR), Pt suffers from sluggish kinetics with activation overpotentials of around 0.3–0.4 V. The durability of Pt/C catalysts under PEMFC conditions is also a matter of concern. The loss in active catalyst surface due to carbon corrosion, Pt dissolution and particle growth is considered to be the major reason for the drop in cell performance with time [3–8]. Besides being influenced by the type of carbon support, Pt dissolution depends on the operating temperature and the potential. A potential of 1.15 V *vs.* RHE at a temperature of 80 °C was found to be the most corrosive [4,9].

Platinum alloyed with transition metals such as Co, Ni, Fe, Cr, Cu, etc. have been extensively studied and found to be at least twice as active as Pt for the ORR [5,10–14]. Amongst others, an electronic effect of the alloy on the Pt surface atoms and the related changes in the Pt–Pt bond distances has been advanced to explain the enhanced ORR. Well-defined Pt_3M (M = Co, Ni, Ti, Fe, V) alloys show enhanced ORR activity due to the formation of a Pt skin following annealing [15–17]. Recent literature also reports that transition metal rich Pt alloys supported on carbon form a core-shell structure after voltammetric dealloying. The specific activity of such dealloyed catalyst was found to be at least a factor of four higher than that of commercially available state-of-the-art Pt catalysts [18–22]. The changes in the Pt–Pt bond distances, commonly coined as geometric strain, due to non-noble metal leaching is considered to influence the reactivity of the surface Pt atoms [23]. The formation of Pt–OH intermediates, which are considered to block the active site for the ORR, is often found to be delayed in Pt alloys, thus enhancing the ORR activity [24]. A general aspect of these studies of Pt alloys is that the catalytic surfaces are enriched in Pt following annealing or dealloying.

The durability of Pt alloys is largely limited by the loss in active surface area due to particle sintering and the dissolution of both Pt and non-noble metal [9,10]. Investigations of Pt-rich and non-noble metal (Co, Ni, Cu, Fe)-rich alloys have stressed the importance

* Corresponding author. Present address: Nedstack Fuel Cell Technology BV, 6802 ED Arnhem, The Netherlands. Tel.: +31 26 3197672.
E-mail address: frank.debruijn@nedstack.com (F.A. de Bruijn).
[1] Present address: Department of Chemistry, NTNU, N-7491 Trondheim, Norway.

0926-3373/$ – see front matter © 2011 Elsevier B.V. All rights reserved.
doi:10.1016/j.apcatb.2011.11.003

of non-noble metal leaching. Typically, the non-noble metal concentration decreases to less than 20 at% after fuel cell operation or electrochemical leaching irrespective of the alloying element and the initial alloy composition [19,20,25,26]. Several studies including our work on PtCo alloys with a wide variation of the initial composition found non-noble metal leaching to be more rapid for non-noble metal rich alloys. This points to the dissolution of metals from the bulk [20,25,26]. The formation of a core-shell structure, spongy Pt particles, percolated and 'swiss-cheese' structures have been reported after acid leaching and electrochemical cycling: while the core-shell structure retains the alloying element in the particle core after leaching, other structures contain only Pt [27–29].

A problem with the use of alloys is that the dissolution of the non-noble metal during fuel cell operation may poison the proton exchange membrane. To prevent such poisoning, such alloys may be pretreated with mineral acids to remove the unalloyed, exposed and excess non-noble metals prior to use in a fuel cell [10].

Accelerated durability studies of electrocatalysts have often been carried out by voltage cycling between high and low potentials mimicking the most corrosive conditions occurring in PEMFC such as during cell start-up/shut-down [9,26,29,30]. Typically, the activity of pure Pt and alloyed Pt electrocatalysts decreases during potential cycling. Contradicting reports exist, however, about the difference in durability between pure Pt and alloyed Pt catalysts, some suggesting a positive effect of alloying on the stability, others indicating that there is no benefit of the alloy [7,29–32].

Most of the Pt alloys synthesis methods employ a high temperature annealing process, which results in a larger average nanoparticle size when compared to the typical particle size of commercially available Pt/C catalyst (~2–3 nm), which often serve as a reference material. It is well known, however, that the intrinsic activity of Pt for the ORR depends on both particle size and shape [33].

Therefore, in this work, efforts were made to compare the activity and durability of Pt and Pt alloys prepared under similar synthesis and annealing conditions. In doing so, carbon supported Pt and Pt alloys with similar particle size and active surface area were obtained and hence the effect of the alloying element on the catalytic activity is systematically determined. Platinum was alloyed with Co, Ni and Cu with two different compositions: one representing a Pt-rich alloy, that is ~$Pt_{75}M_{25}$/C and the other one a non-noble metal-rich composition, i.e. ~$Pt_{20}M_{80}$/C. Pt/C with a variety of particle sizes were formed by annealing at three different temperatures such as 350 °C, 600 °C and 950 °C while Pt alloys were prepared by annealing at 350 °C and 950 °C.

The non-noble metals from the alloys were partially removed by brief electrochemical dealloying at room temperature. Thereafter, stability tests were carried out at 80 °C, this being the operating temperature of a PEMFC. The durability of the catalysts was investigated with respect to the surface area loss, the particle growth and the Pt:M atomic composition change as a function of potential cycling. The bulk composition was determined by EDS, the particle size by TEM and phase identification was carried out by XRD. The affinity of the electrode surface for O(H) was gauged by the potential of the PtO_x reduction peak in the cyclic voltammogram.

2. Experimental

2.1. Carbon pretreatment

Vulcan XC-72R (Cabot) is used as the carbon support in this work. Prior to catalyst preparation the carbon support was pretreated in 3 M HNO_3 for 8 h at 120 °C. The carbon powders were then filtered, extensively washed with Millipore water (18 MΩ cm) and dried overnight in an oven at 120 °C.

2.2. Catalyst preparation

The metal salts $H_2PtCl_6{\cdot}6H_2O$, $Ni(NO_3)_2{\cdot}6H_2O$, $Co(NO_3)_2{\cdot}6H_2O$ and $Cu(NO_3)_2{\cdot}3H_2O$ (all from Sigma–Aldrich, ACS reagent) were used as precursors for the preparation of Pt and Pt alloys. All the catalysts prepared in this study have a Pt loading of 10 wt% with respect to the carbon support and, therefore, a variable loading of non-noble metal. Appropriate amounts of the metal salt precursors were dissolved in water and a known quantity of pretreated carbon powdered was added to the solution. The resulting suspension was stirred for 3 h before drying in an oven at 120 °C for 3 h. The catalyst precursors were then powdered and reduced under H_2/Ar (10% H_2) atmosphere at various temperatures to study the phase change and the crystallite size effect. While Pt-only precursors were annealed at 350 °C, 600 °C and 950 °C, Pt alloy precursors were annealed at 350 °C and 950 °C.

To carry out electrochemical experiments, the catalysts were deposited on an Au rotating disk electrode (RDE). To this end, 200 μl of Millipore water was added to 5 mg of the carbon supported alloy powder and ultrasonicated for 1 h [34]. The mixture was then stirred continuously using a magnetic stirrer with a Teflon magnetic pellet for two days to form the catalyst ink. 10 μl of the ink, which amounts to a Pt loading of around 55–90 μg cm^{-2} depending on the catalyst, was then casted on a polished Au RDE and dried at 75 °C for 2 h. The electrode was then cooled to room temperature before introduction in the electrochemical cell.

2.3. Determination of composition

EDS analysis was carried out using a Quanta 3D FEG instrument (FEI) to determine the bulk Pt:M atom ratios of the fresh and aged alloys. To determine the composition of fresh alloys the fresh catalyst powders were dispersed directly on the substrate holder. However, the aged alloys were characterized by mounting the catalyst coated Au substrate on the substrate holder immediately after the electrochemical measurements. Various spots were selected for determining the elemental composition. The reported compositions are averages of the spot analyses.

The surface elemental composition of selected samples (non-noble metal-rich alloys annealed at 950 °C) after 1000 CV scans at 80 °C was analyzed using a Kratos AXIS Ultra X-ray Photoelectron Spectrometer, equipped with a monochromatic Al Kα X-ray source and a delay-line detector (DLD). Spectra were obtained using the aluminum anode (Al Kα, 1486.6 eV) operating at 150 W with survey and region scans at constant pass energies of 160 eV and 40 eV, respectively. Depth profiles were obtained by sputtering, while rotating the sample using an Ar pressure of 3×10^{-8} mbar. The emission current was set to 15 mA with a beam energy of 4 kV.

2.4. Structural and phase analysis

X-ray diffraction patterns for the catalysts were recorded using a Bruker D4 Diffractometer to verify alloy formation. The JCPDS powder diffraction database was used as reference for analysis of the XRD patterns.

The lattice constant of Pt and the alloying element in different phases was determined by deconvolution and peak fitting. The composition of the alloys in each phase is then estimated from Vegard's law, $(1-x)a_1 + xa_2 = a$, with x being the molar fraction of the solute element, a_1 the lattice constant of the pure solvent, a_2 the lattice constant of the pure solute and a the measured lattice constant of the formed alloy.

2.5. Electrochemical characterization

Before casting the catalyst ink on the Au RDE, the RDE was electrochemically cleaned in 0.5 M H_2SO_4 by scanning between 0

and 1.7 V at a scan rate of 50 mV/s until a stable CV was obtained. A three-compartment electrochemical cell was used with a platinized platinum counter electrode and a lab-made RHE. The temperature of the whole electrochemical cell was controlled using a thermostat.

Initially, all the catalysts were potentially cycled for 25 CV scans in 0.5 M $HClO_4$ within the potential range between 0.02 and 1.3 V and at a scan rate of 50 mV/s at room temperature under Ar atmosphere. These initial CVs were made to obtain a relatively stable surface and to follow the initial dealloying process. The temperature of the cell was then increased to 80 °C and the catalysts were electrochemically scanned for another 1000 CV scans between 0.6 and −1.2 V at a scan rate of 100 mV/s under Ar atmosphere to study their durability.

The ORR activity of the catalysts was measured by scanning the electrodes between the potential of 1.1 V and 0.2 V in oxygen-saturated 0.5 M $HClO_4$ at a scan rate of 5 mV/s. The supply of oxygen was maintained throughout the measurement to keep its concentration in solution constant. The rotating speed was set at 1600 rpm.

2.6. Particle size analysis

The particle size of a subset of the alloys was analyzed by use of a Tecnai Sphera transmission electron microscope (FEI Company) operated at a voltage of 200 kV. The catalysts were dispersed in ethanol and ultrasonicated for a few seconds before being mounted on a carbon coated Cu grid. The grid was dried at room temperature and then introduced into the sample holder. For PtCu/C alloys, carbon coated Mo grids were used instead.

3. Results and discussion

3.1. Characterization of fresh catalysts

The main techniques used to characterize Pt/C and PtM/C catalysts are XRD and TEM. The XRD patterns are collected in Fig. 1, while the TEM data of a few catalysts are illustrated in Fig. 2 (for the rest of the catalysts, refer to Fig. S1 of Supplementary data). The phase compositions and particle sizes derived from them are presented in Table 1, to which continuous reference will be made. The alloy compositions determined with EDS are close to the compositions aimed at in the preparation process.

3.2. Formation of Pt/C and PtM/C alloys

The XRD patterns of the Pt/C catalysts reduced/annealed at 350, 600, and 950 °C are shown in Fig. 1a (bottom). Clearly, as expected, the diffraction peaks sharpen up as the reduction temperature increases, indicating Pt particle growth. Application of the Scherrer equation gave for the average particle size values of 2, 6, and 13.8 nm, respectively. These values were checked against TEM (Supplementary Fig. S1), which gave lower numbers in the last two cases (Table 1), but the agreement is reasonable.

The XRD patterns of the two different PtCo/C alloys annealed at 350 and 950 °C are also shown in Fig. 1a (top). A shift in the diffraction peaks of $Pt_{75}Co_{25}$/C towards higher degree 2θ when compared to pure Pt is caused by the lattice contraction of Pt with the substitution of smaller Co atoms for the larger Pt atoms. Again, sharper diffraction peaks for the $Pt_{75}Co_{25}$/C annealed at 950 °C indicate that grain growth is favored at higher annealing temperatures.

A single-phase PtCo alloy is not achieved for $Pt_{20}Co_{80}$/C when annealed at 350 °C. The diffraction peaks seen in Fig. 1a for this alloy show the presence of Coin the hcp phase. As no diffraction peak for Pt is noticed for this alloy it is concluded that the Pt is completely alloyed with Co. The shoulder in the region of the Pt(1 1 1) peak reveals the formation of a Pt-rich fcc PtCo phase. However, $Pt_{20}Co_{80}$/C when reduced under H_2 at 950 °C yields a single fcc phase similar to the $PtCo_3$ structure, although a small amount of unalloyed Co is still present. From the lattice constants of 3.85 and 3.58 Å derived for completely alloyed $Pt_{75}Co_{25}$/C and $Pt_{20}Co_{80}$/C, respectively, the Pt:Co phase compositions of 81:19 and 15:85 were obtained with Vegard's law, in satisfactory agreement with EDS.

Unlike for $Pt_{75}Co_{25}$/C annealing of $Pt_{75}Ni_{25}$/C at 350 °C did not lead to a single phase. Instead, from Fig. 1b it is concluded that the alloy contains PtNi in two fcc phases: one is a pure Pt phase and the

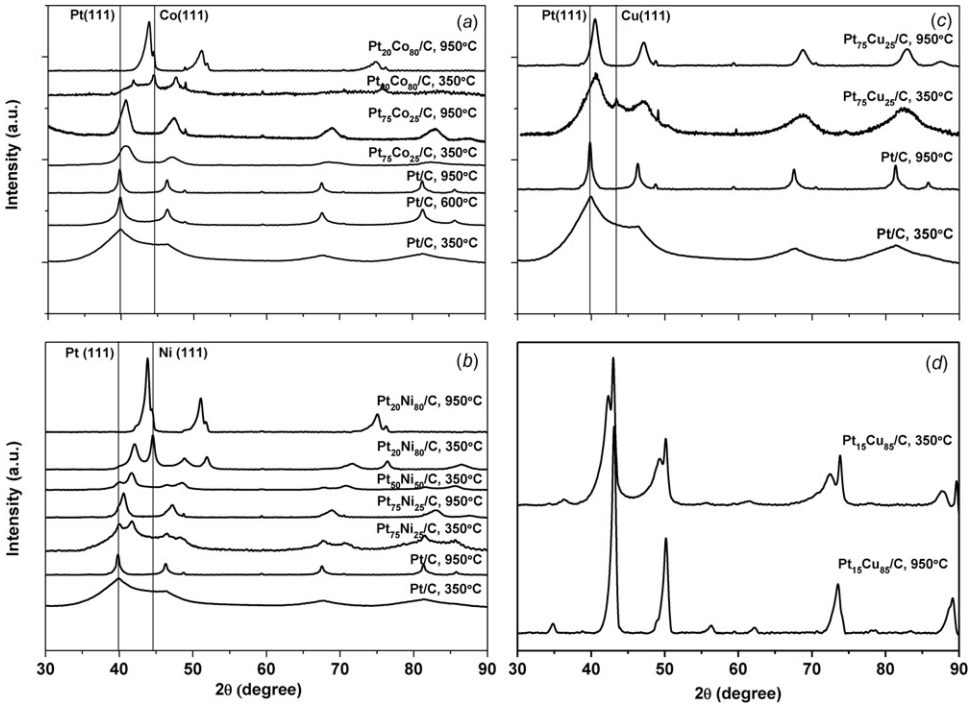

Fig. 1. XRD patterns of (a) fresh Pt/C and PtCo/C, (b) PtNi/C, (c) Pt-rich PtCu/C and (d) Cu-rich PtCu/C at various annealing temperatures.

Table 1
Table showing the results of compositional, structural and morphological analysis of the catalysts.

Catalyst (EDS based composition)	Anneal. temp. (°C)	Pt:M composition, XRD	Lattice constant, a (Å)	Crystallite size, d_{XRD} (nm)	Particle size fresh, d_{TEM} (nm)	Particle size aged, d_{TEM} (nm)
Pt/C	350	100:0	3.92	2	2.3 ± 0.8	6 ± 3
Pt/C	600	100:0	3.92	6	4 ± 1	7 ± 2
Pt/C	950	100:0	3.92	13.8	9 ± 2	11 ± 3
$Pt_{75}Co_{25}$/C	350	81:19	3.85	4.3	3 ± 1	7 ± 2
$Pt_{75}Co_{25}$/C	950	81:19	3.85	7.2	6 ± 2	7 ± 2
$Pt_{20}Co_{80}$/C	350	–	–	–	4 ± 2	9 ± 2
$Pt_{20}Co_{80}$/C	950	15:85/–	3.58/3.54	9.2	9 ± 2	10 ± 2
$Pt_{75}Ni_{25}$/C	350	100:0/60:40	3.92/3.75	3.5/5.4	3 ± 1	–
$Pt_{75}Ni_{25}$/C	950	80:20	3.84	8.3	10 ± 3	11 ± 3
$Pt_{50}Ni_{50}$/C	350	100:0/60:40	3.91/3.75		–	–
$Pt_{20}Ni_{80}$/C	350	50:50/0:100	3.72/3.52	5.7/13	–	–
$Pt_{20}Ni_{80}$/C	950	12:88/–	3.57/3.53	13	8 ± 3	9 ± 3
$Pt_{75}Cu_{25}$/C	350	81:19	3.86	3	3 ± 1	8 ± 2
$Pt_{75}Cu_{25}$/C	950	77.5:22.5	3.85	9.2	10 ± 3	10 ± 3
$Pt_{15}Cu_{85}$/C	350	Fm-3m 23:77 Pm-3m 10:90	Fm-3m 3.68 Pm-3m 3.64	5.4/6	6 ± 1	7 ± 2
$Pt_{15}Cu_{85}$/C	950	Pm-3m 10:90	Pm-3m 3.64	11.7	8 ± 1	8 ± 3

d_{XRD} of HiSPEC™ 4000 (40% Pt on Vulcan XC-72R) = 4.5 nm.

other one characterized by a peak at $2\theta = 41.7^\circ$ corresponding to a PtNi phase with a 60:40 Pt:Ni ratio. PtNi alloys with an even higher Ni content of around 50 and 80 at% were prepared and annealed at 350 °C to study the formation of different PtNi alloy phases. Fig. 1b shows that the amount of the pure Pt fcc phase decreases with increasing Ni content. The shift of the peak characteristic for PtNi to a higher angle when the Ni content was around 80 at% points to the increasing Ni content of the alloy phase. The computed Pt:Ni composition of this phase is 50:50.The presence of a diffraction peak at $2\theta = 44.6^\circ$ for $Pt_{20}Ni_{80}$/C at 350 °C is indicative of the presence of a

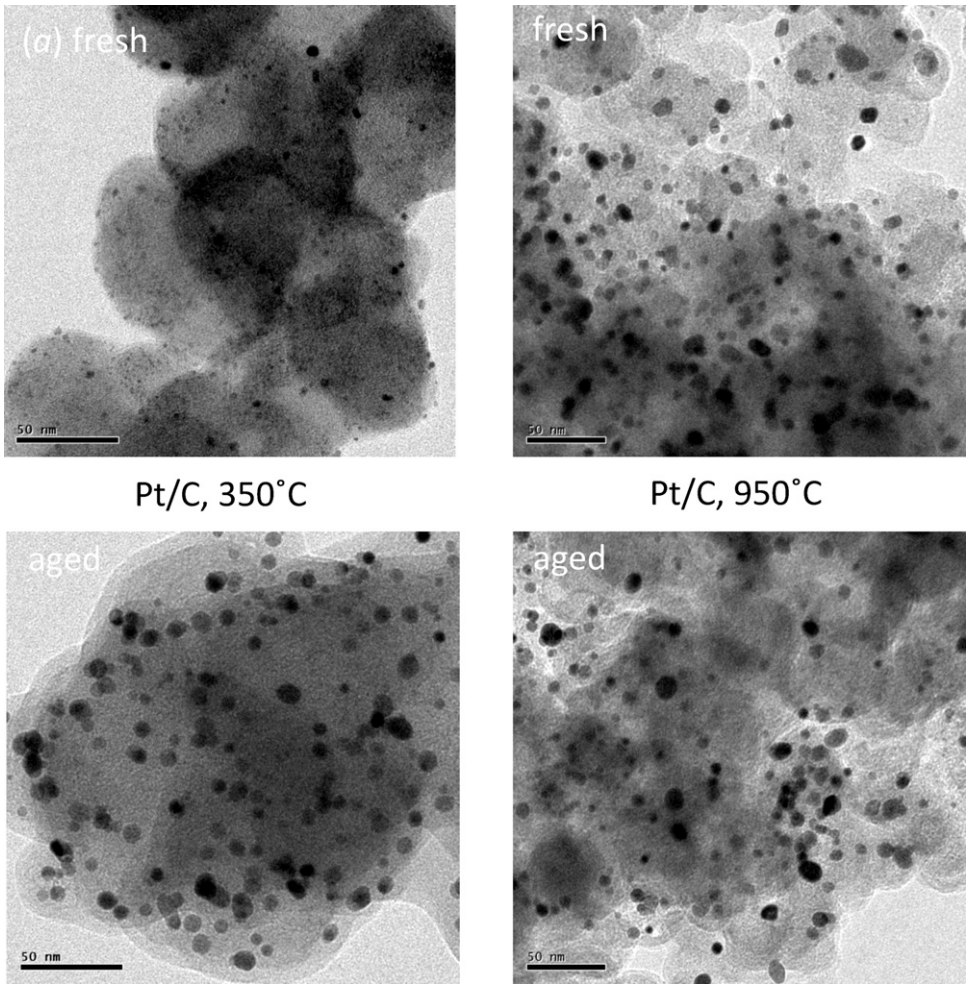

Fig. 2. TEM images of (a) Pt/C (350 °C and 950 °C), (b) Pt-rich PtCu/C (350 °C and 950 °C) and (c) Cu-rich PtCu/C (350 °C and 950 °C) fresh and aged catalysts.

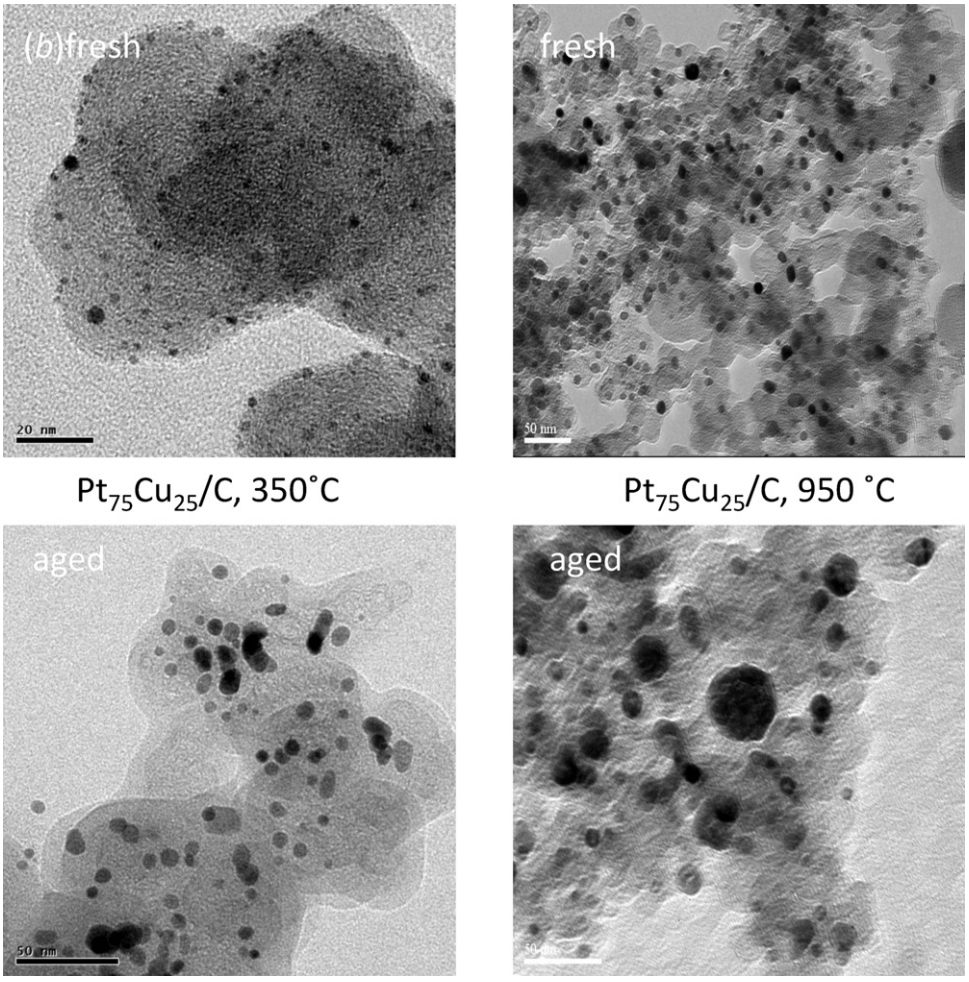

Fig. 2. (*Continued*)

pure Ni fcc phase. This phase was not observed for the alloys with a lower Ni content.

The $Pt_{75}Ni_{25}$/C and $Pt_{20}Ni_{80}$/C alloys annealed at 950 °C contained a single alloy phase similar to what was found for $Pt_{75}Co_{25}$/C and $Pt_{20}Co_{80}$/C annealed at the same temperature. For $Pt_{20}Ni_{80}$/C the peak of pure fcc Ni phase shifts slightly towards lower 2θ values, which can be taken as an indication of the expansion of the Ni lattice due to the dispersion of Pt into its lattice. The lattice constant and the Pt:Ni atomic phase composition of the alloyed phases in $Pt_{75}Ni_{25}$/C and $Pt_{20}Ni_{80}$/C are found to be 3.84 Å and 3.57 Å and 80:20 and 12:88 respectively.

The amount of unalloyed non-noble metal in the case of $Pt_{20}Co_{80}$/C and $Pt_{20}Ni_{80}$/C annealed at 950 °C is very low compared to the alloys with similar compositions annealed at 350 °C. Thus, the application of higher annealing temperatures facilitates alloy formation by the diffusion of atoms but also leads to sintering as evident from the much larger particles (Table 1). Overall, disordered single-phase PtCo and PtNi alloys with a very high Co and Ni concentration of ~80 at% could be achieved by straightforward impregnation followed by annealing.

Annealing of $Pt_{75}Cu_{25}$/C alloy was done at 350 and 950 °C and led to alloys as evident from the shift in the Pt(1 1 1) peak towards higher angles (Fig. 1c). After annealing of $Pt_{15}Cu_{85}$/C at 350 °C no single phase alloy was formed (Fig. 1d). Instead a Cu-rich disordered fcc(Fm-3m) phase with sharp peaks at $2\theta = 42.3°$, 49.3°, 72.4° and 87.7° and a Cu-rich ordered cubic (Pm-3m) structure with strong diffraction peaks at $2\theta = 43°$, 50°, 73.6° and 89.6° and weak diffraction peaks at $2\theta = 34°$, 56°, 61.5° and 78° were identified by XRD. Composition analysis with Vegard's law revealed a Pt:Cu atom ratio of 10:90 for the ordered phase with a lattice constant of 3.64 Å and a ratio of 23:77 for the disordered phase with a lattice constant of 3.68 Å. The crystallite size of the former ordered phase is found to be higher than that of the relatively lower Cu content disordered phase by application of the Scherrer equation.

Fig. 1d shows that the amount of ordered PtCu phase increased upon annealing $Pt_{15}Cu_{85}$/C at 950 °C while the disordered phase almost completely disappeared. The lattice constant and Pt:Cu atom ratio was 3.64 Å and 10:90, respectively, for this composition. However, the presence of a shoulder at $2\theta = 49°$ along with some asymmetry in the strong diffraction peaks suggest the presence of a trace amounts of an alloy with the disordered fcc structure.

The emergence of partially ordered and disordered structures for Cu-rich PtCu alloys when annealed at 800 °C in hydrogen has been reported before [18]. The ordered phase was found to be richer in Cu than the disordered phase. Similarly, Mani et al. obtained a disordered fcc structure with an unalloyed pure Cu phase upon annealing at 600 °C and 950 °C [19]. A closer look at their XRD data confirms the emergence of an ordered phase with increasing annealing temperature, although this detail is not discussed in their paper. However, in our case, depending on the annealing temperature a partially ordered and a completely ordered Cu-rich PtCu alloy were formed, the atomic Pt:Cu ratio being 10:90 in the completely ordered phase in both cases.

As in the Pt/C case, also for the alloys the average particle size has been estimated both from the XRD line width (Scherrer equation) and from the transmission electron micrographs. The results

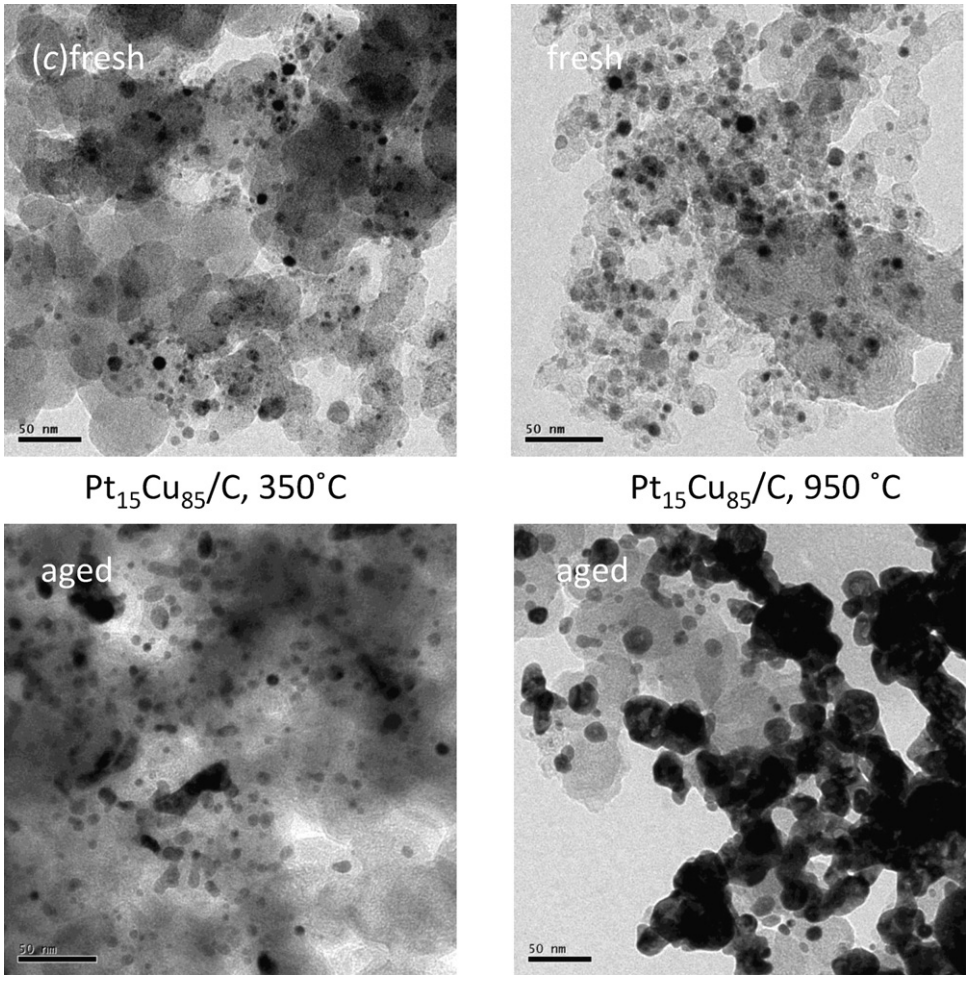

Fig. 2. (*Continued*).

are presented in Table 1, and it is seen that (i) there is satisfactory agreement between the two sets of data, (ii) the range of particle sizes is similar to the one observed for Pt, although at 350 °C the alloy particle sizes tend to be somewhat greater than that of Pt, and (iii) that, independent of the reduction temperature, the crystallite sizes of the Pt-rich alloys are smaller than that of the non-noble metal-rich ones. In the cases where two phases were present, the average particle size could be evaluated from the XRD data: they also conform to conclusion (iii) above.

3.3. Electrochemical characterization at room temperature

3.3.1. Cyclic voltammetry

It took about 25 cycles (0.02–1.3 V) for all the electrocatalysts to stabilize. The changes in CV profile were of course most drastic for the non-noble metal rich alloys. This is documented in Fig. 3a–c, pertaining respectively to $Pt_{20}Co_{80}$/C, $Pt_{20}Ni_{80}$/C, and $Pt_{15}Cu_{85}$/C (all annealed at 950 °C), showing strong dissolution of the non-noble component in the first few cycles. The dissolution of Cu appears to take place in two steps (Fig. 3c): the peak at 0.35 V corresponds to the dissolution of bulk Cu, while the peak at around 0.8 V is ascribed to the dissolution of Cu from a Pt environment. In the case of the Ni- and Co-containing catalysts, only one dissolution peak is visible, at 0.4–0.5 V, which presumably corresponds to the removal of non-noble metal from the alloy (E^0 (M/M^{2+}) being too low to observe bulk dissolution here).

The stable CV profiles of Pt and the Pt–M alloys at room temperature are given in Fig. 4. For Pt/C (Fig. 4a) it is clear that increasing the annealing temperature leads to a better defined hydrogen ad- and desorption region, with a clear distinction between the ~0.1 and ~0.25 V peaks, which can be ascribed to Pt(1 1 0) and Pt(1 0 0) facets, respectively [27]. This of course tallies with the particle growth concomitant with an increase in annealing temperature, leading to better defined particles with less edge and corner atoms. It is also reflected in the gradual shift of the PtO_x reduction peak to higher potentials (larger Pt particles are less easily oxidized and have lower oxygen affinities). This peak appears to be broader for catalysts annealed at the lower temperatures, possibly also reflecting a larger particle size distribution.

Broadly speaking the same observations can be made for the Pt-rich alloys, albeit with some qualifications as far as the H_{upd} region is concerned. $Pt_{75}Ni_{25}$ (Fig. 4c) tracks Pt the closest, while interpretation of $Pt_{75}Co_{25}$ (Fig. 4b) and $Pt_{75}Cu_{25}$ (Fig. 4d) is somewhat hampered by H_2 evolution/oxidation at low potentials, especially for the catalysts annealed at 950 °C. This is in itself interesting, since the three non-noble metals do not differ much in M–H bond strength. Nevertheless, it would seem that the Pt signature does appear after the high-temperature anneal, although the distinction between the Pt(1 1 0) and Pt(1 0 0) peaks is not so clear as it was for Pt/C.

For the non-noble metal rich alloys, the CV after the low-temperature anneal is not so different from that of the Pt-rich alloys, but a high temperature anneal does not bring forth the typical Pt features very clearly, although they do tend in that direction. Due to the strong dissolution of the non-noble metal component it stands to reason that these initially non-noble metal rich alloys

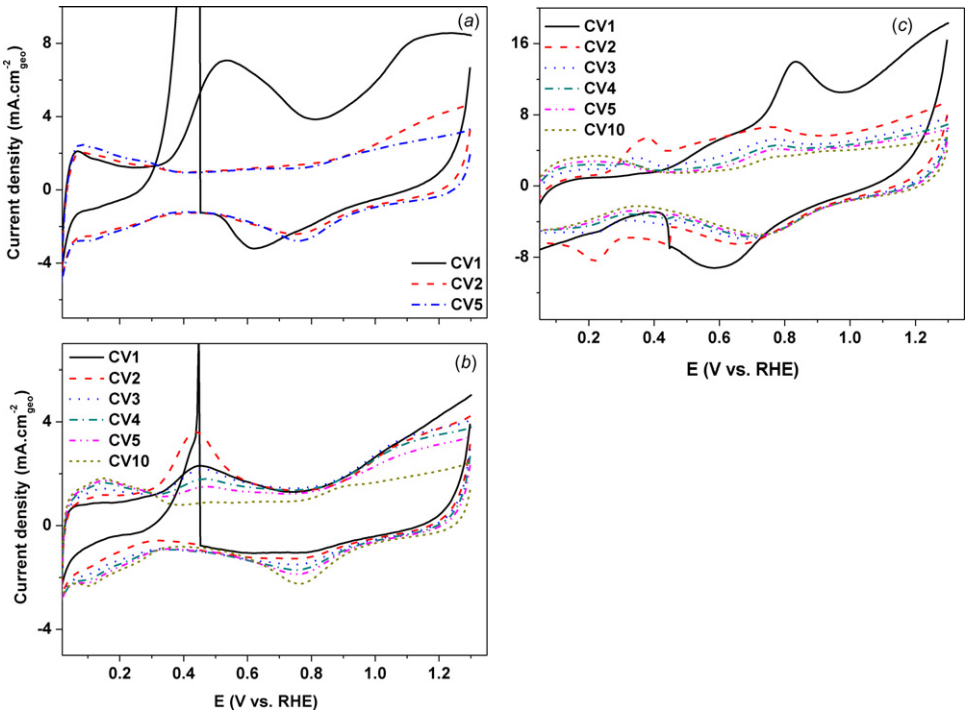

Fig. 3. Initial CV profiles of (a) $Pt_{20}Co_{80}$/C, (b) $Pt_{20}Ni_{80}$/C and (c) $Pt_{15}Cu_{85}$/C formed at 950 °C showing the dealloying of non-noble metal at room temperature; conditions: 0.5 M $HClO_4$, 50 mV/s, Ar atmosphere.

will look rather different after 25 CVs from the fresh catalyst, so that a clearly resolved H_{upd} region was perhaps also not to be expected. The broad redox peak at about 0.4–0.5 V is due to oxygen-containing surface groups ((hydro) quinone-like) on the carbon support.

As mentioned above for Pt/C, the position of the Pt oxide reduction peak varies with the particle size. For the alloys, given that the particle sizes of the 350 °C annealed PtM/C catalysts are smaller than those of the 950 °C annealed ones (Table 1), the same conclusion appears evident from an inspection of Fig. 4b–d. However, a closer look at the data indicates that the relation between particle size and PtO_x reduction peak potential is only a rough one (Fig. 5), and, moreover, that there are no consistent differences between alloys containing Co, Ni, or Cu.

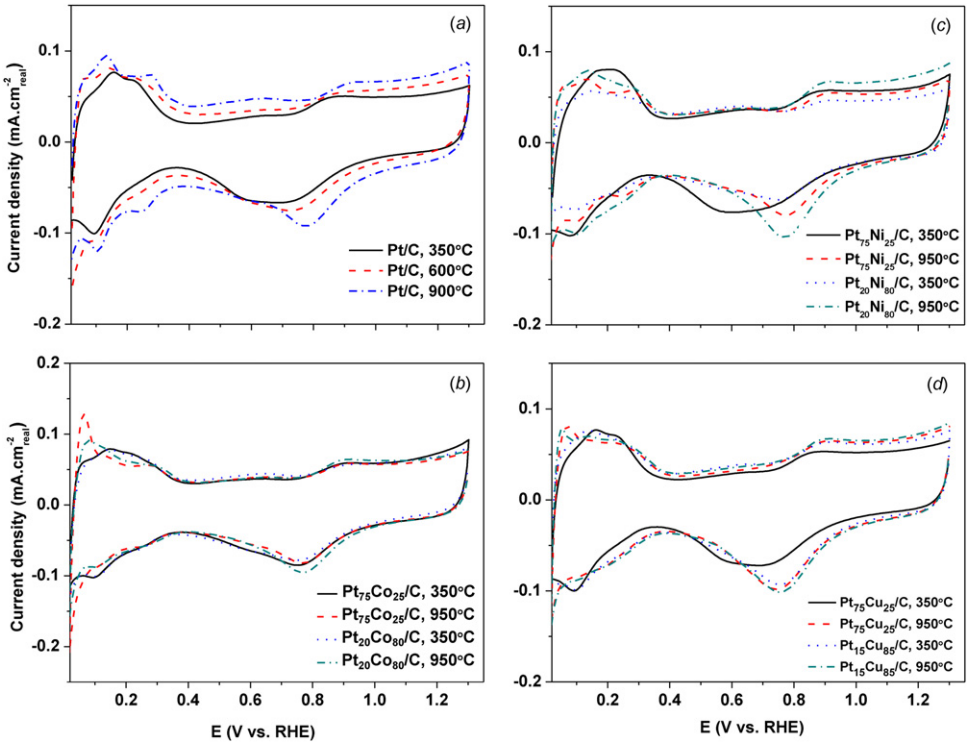

Fig. 4. CV profiles of (a) Pt/C, (b) PtCo/C, (c) PtNi/C and (d) PtCu/C after 25 CV scans at room temperature; conditions: 0.5 M $HClO_4$, 50 mV/s, Ar atmosphere.

Table 2
Electrochemical data derived from the accelerated durability experiments.

Catalyst	Anneal. temp. (°C)	Specific surface area (m^2 g_{Pt}^{-1})		Half-wave potential, $E_{1/2}$ (mV)		% ECSA retained
		25@RT	5@80C	25@RT	1000@80C	1000@80C
Pt/C	350	106	97	877	882	43
Pt/C	600	52	71	888	853	38
Pt/C	950	35	55	870	867	49
$Pt_{75}Co_{25}$/C	350	72	65	895	877	62
$Pt_{75}Co_{25}$/C	950	86	81	905	881	83
$Pt_{20}Co_{80}$/C	350	51	51	895	878	74
$Pt_{20}Co_{80}$/C	950	72	67	921	878	79
$Pt_{75}Ni_{25}$/C	350	109	96	881	875	43
$Pt_{75}Ni_{25}$/C	950	64	65	896	874	59
$Pt_{20}Ni_{80}$/C	350	29	46	881	872	62
$Pt_{20}Ni_{80}$/C	950	53	76	912	889	56
$Pt_{75}Cu_{25}$/C	350	108	108	880	879	40
$Pt_{75}Cu_{25}$/C	950	54	51	894	876	47
$Pt_{15}Cu_{85}$/C	350	70	79	919	873	59
$Pt_{15}Cu_{85}$/C	950	41	48	931	890	63

As the amount of Pt present in the electrode is known, the specific Pt surface area (SSA) of the catalysts could be calculated from the charge under the hydrogen underpotential deposition region. It is assumed that in these first 25 cycles at room temperature no Pt has been lost due to dissolution. Thus, the derived numbers are listed in Table 2. Comparing these data with the particle sizes in Table 1, one can certainly conclude that catalysts with very small particles show higher values for the SSA than those with large particles, as they should, but, again, the correlation is not very precise.

3.3.2. Alloy composition after 25 CVs

EDS was employed to determine the Pt:M ratio in the stabilized Pt alloys annealed at 950 °C. $Pt_{20}Ni_{80}$/C, $Pt_{20}Co_{80}$/C and $Pt_{15}Cu_{85}$/C contained 55, 45 and 20 at% of non-noble metal, respectively, after the initial stabilization for 25 CV scans. The greater leaching of Cu is in line with the results obtained for PtM electrodeposits [35]. The more pronounced segregation of Pt to the surface of PtCo and PtNi alloys is argued to limit non-noble metal dissolution [20] and is in line with the lower segregation noted for PtCu alloys [31,32]. In the case of Pt-rich alloys, a non-noble metal content of about 15–20 at% was retained, which is again quite similar to the electrodeposits case.

3.3.3. ORR activity

The ORR polarization curves of selected catalysts (PtCo group) in oxygen-saturated electrolyte are shown in Fig. 6, while that of the other catalysts are shown in Supplementary Fig. S2. The half-wave potentials ($E_{1/2}$) derived from these plots are listed in Table 2. They seem to indicate already that quite a few of the alloy catalysts are more active than their Pt-only counterparts. To be more precise, the specific activity of the catalysts was determined at 0.9 V by dividing the observed kinetic current at that potential by the Pt electrochemical surface area (ECSA) after 25 CV scans. The resulting numbers are given in Table 3. Clearly, as has been observed many times before, the specific activity for Pt/C depends on the Pt particle size, increasing with decreasing size [36,37]. Generally speaking, the same appears to hold for PtM/C: annealing at 950 °C, which generates the larger particles, leads to catalysts with a higher specific activity than annealing at 350 °C. This alloy particle-size dependency of the specific activity has also been observed before, for PtCo/C [34].

To aid in a more precise comparison between Pt and the alloy catalysts, the specific activities calculated at 0.9 V are plotted against the TEM particle size of the fresh catalysts in Fig. 7. There is quite some apparent scatter, but it appears safe to conclude that

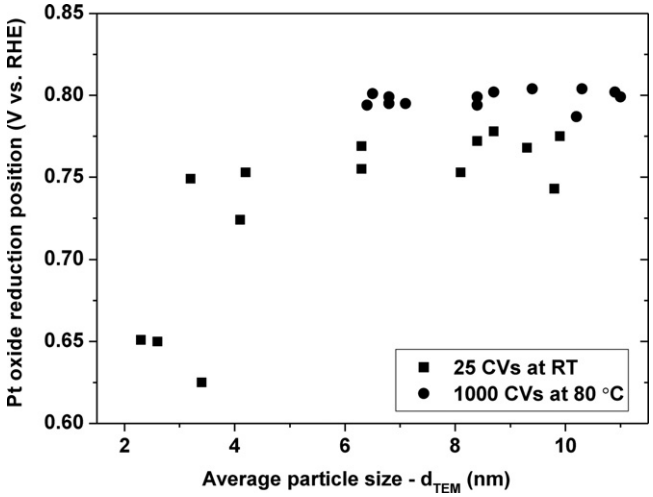

Fig. 5. Platinum oxide reduction potential as a function of particle size (d_{TEM}) after (■) 25 CVs at room temperature and (●) 1000 subsequent CVs at 80 °C.

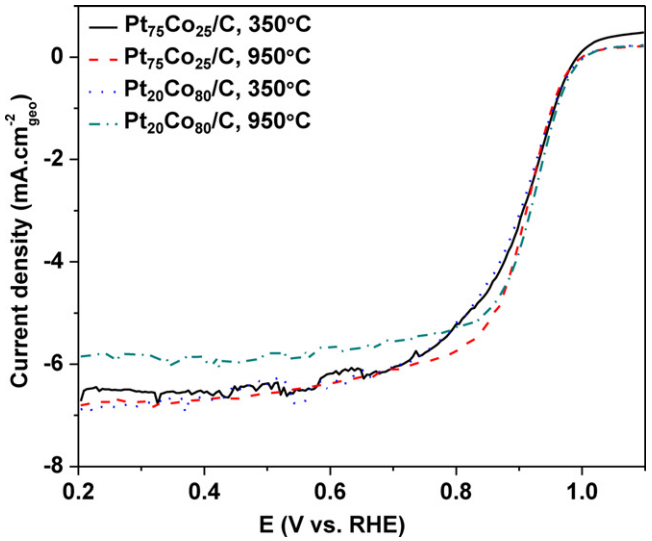

Fig. 6. ORR polarization curves of PtCo/C alloys after 25 CV scans at room temperature; conditions: 0.5 M $HClO_4$, 5 mV/s, O_2 atmosphere, 1600 rpm.

Table 3
Specific activity and mass activity of the catalysts during the durability tests.

Catalyst	Anneal. temp. (°C)	Specific activity at 0.9 V ($\mu A\,cm_{Pt}^{-2}$)		Mass activity at 0.9 V ($mA\,mg_{Pt}^{-1}$)
		25@RT	1000@80C	25@RT
Pt/C	350	37	64	39
Pt/C	600	98	59	50
Pt/C	950	152	114	52
$Pt_{75}Co_{25}$/C	350	91	78	65
$Pt_{75}Co_{25}$/C	950	236	127	203
$Pt_{20}Co_{80}$/C	350	214	133	109
$Pt_{20}Co_{80}$/C	950	414	143	238
$Pt_{75}Ni_{25}$/C	350	35	63	39
$Pt_{75}Ni_{25}$/C	950	226	102	145
$Pt_{20}Ni_{80}$/C	350	163	117	–
$Pt_{20}Ni_{80}$/C	950	318	127	168
$Pt_{75}Cu_{25}$/C	350	56	78	61
$Pt_{75}Cu_{25}$/C	950	430	108	210
$Pt_{15}Cu_{85}$/C	350	252	87	177
$Pt_{15}Cu_{85}$/C	950	434	127	178
40% Pt/C*		91	71	

* HiSPEC™ 4000 (40% Pt on Vulcan XC-72R).

most of the small-particle, 350 °C annealed catalysts do not show an improved performance with respect to Pt itself with PtCo being a clear exception in this case, but that at the higher particle sizes, some PtM catalysts are better than Pt by a factor of ~2.5. The PtCu and PtCo catalysts as a group appear to be the best performers. Meanwhile, of the 950 °C annealed catalysts, the non-noble metal-rich alloys perform better than their Pt-rich counterparts except $Pt_{75}Cu_{25}$/C, which shows high activity similar to that of the non-noble metal-rich alloys.

It might perhaps be argued that it would be better to try and correlate the specific activity with the SSA determined just previously to the ORR measurements. Unfortunately, this does not improve the situation very much: the apparent scatter is even increased, although now almost all alloy catalysts are better than their Pt counterparts, by a factor of up to nearly 4. There is no clear relation between the PtO_x reduction peak potential and ORR performance, a conclusion that was also reached in the case of electrodeposits [35]. As to the influence of the phase purity, it is clear that it is dominated by the particle-size effect. In particular, a lower than expected specific activity, on the basis of the activity *vs.* particle size correlation, cannot be systematically traced to the alloy catalyst being biphasic instead of single phase. The reason for this state of affairs is presumably that due to the extensive dissolution of the non-noble metal component during the stabilization period, the precise starting composition does not in general matter all that much.

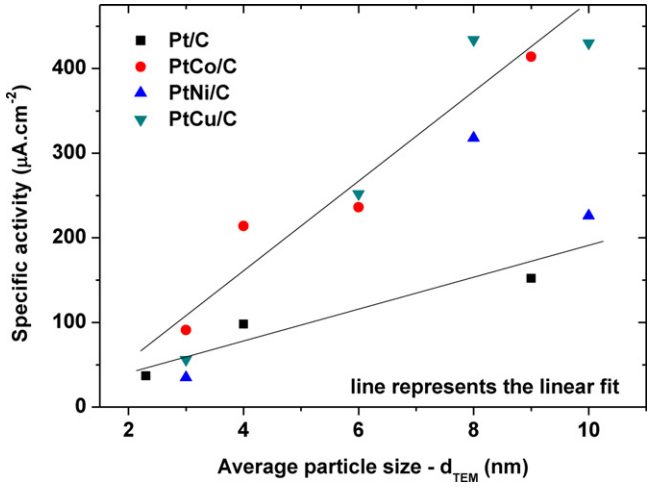

Fig. 7. Specific activity of the catalysts at 0.9 V as the function of particle size (d_{TEM}) before the durability tests at 80 °C: (■) Pt/C, (●) PtCo/C, (▲) PtNi/C and (▼) PtCu/C.

The mass activity (A/g_{Pt}), a measure of the amount of Pt required in a fuel cell, is very relevant in a practical perspective. The respective mass activities shown in Table 3 indicate that, among the catalysts reduced at high temperature, Pt alloys reveal about 3–4.5 times higher mass activity with respect to Pt. The catalysts with the lower particle size (<3.5 nm) possess the lowest mass activity of all the catalysts with Pt alloys showing about 1.5 times higher mass activity than Pt.

3.4. Durability of the catalysts

All the catalysts listed in Table 2 have been subjected to the 1000 CV scan durability test at 80 °C. The final cyclic voltammograms are shown in Fig. 8.

Roughly speaking, the CV profiles of all the catalysts look rather similar, although one might observe that the H_{upd} region of 350 °C annealed Pt/C and $Pt_{75}Ni_{25}$/C appears to be somewhat less structured than that of the others. Compared with 25 cycles at room temperature, the carbon support redox feature near 0.6 V does appear to be greater in intensity. Moreover, the increase in the oxidation current from 1.1 V definitely suggests that the carbon corrosion is indeed severe with the voltage cycling at 80 °C. It has already been established that of the oxygen-containing carbon groups only (hydro)quinone-like groups are electrochemically active and they represent only a small percentage out of all the oxygenated species[38]. Again, the different alloys do not have a distinct influence on the intensity of this carbon redox feature or the CO_2 evolution current – and as the carbon loss was not measured, it is not really clear whether this means that the carbon oxidation is not catalyzed by Pt and its alloys, or that all alloys have a comparable effect on this oxidation, or that the voltammetric signature is not a good guide to carbon support degradation.

The platinum oxide reduction peak of all the catalysts has shifted towards more anodic potential after the durability test, indicating an increase in particle size due to ageing. The shift was more important for the catalysts having lower initial particle size, such that the reduction peak potential ended up being much the same for all the catalysts. To check on the Pt (alloy) sintering behavior, the spent catalysts were re-examined with TEM. The resulting micrographs of selected catalysts are exemplified in Fig. 2 and Supplementary Fig. S1, where they can easily be compared with the fresh ones. In

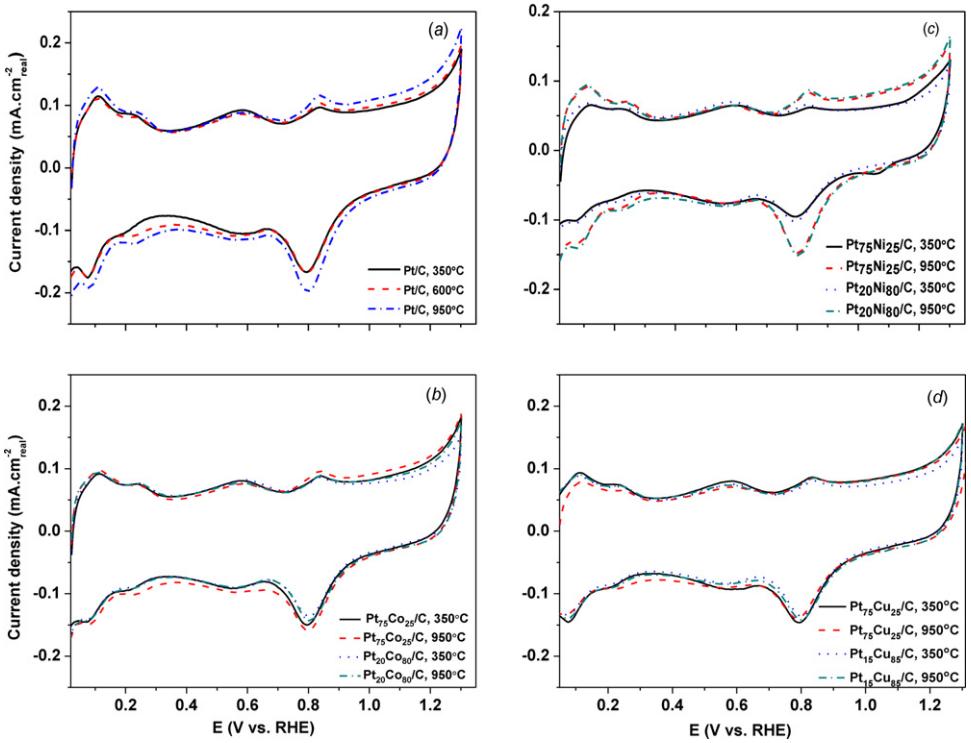

Fig. 8. CV profiles of (a) Pt/C, (b) PtCo/C, (c) PtNi/C and (d) PtCu/C after 1000 CV scans at 80 °C; conditions: 0.5 M $HClO_4$, 50 mV/s, Ar atmosphere.

agreement with the above, particle growth is clearly evident for the catalysts with lower initial particle size. All in all, however, it is rather difficult to analyze these micrographs because of particle coalescence (to be counted as one, or several particles?), and, more problematically, in the case of non-noble metal rich alloys, the formation of so-called percolated structures (Fig. 2c). These structures have been argued to be formed if the initial non-noble metal content of the alloy exceeds 60 at%, leaching of which would lead to "spongy" particles that could collect in such a percolated structure [29]. However that may be, the particle sizes of the aged catalysts reported in Table 1 have been based on the single spherical particles that could be found, and, therefore, presumably represent the lower limit of the real particle size distributions. In Fig. 5 the Pt oxide reduction peak potential is plotted *vs.* the average particle size, both for the fresh and the 80 °C aged catalysts. Two conclusions obtrude themselves: (i) all the low particle sizes have increased to at least 6 nm, and (ii) the scatter in the peak potential values is much smaller after ageing than before it.

The alloy composition of the aged 950 °C annealed catalysts was determined by EDS to find out how much of the non-noble metal was retained in the catalysts. It turns out that only 5–10 at% was left, irrespective of the initial non-noble metal content. This indicates that the durability test is more severe for the PtM/C catalysts that for the corresponding PtM electrodeposits, which retained about 2 times this amount of non-noble metal [35].

A general growth of the Pt (alloy) particles should of course also be reflected in a loss of Pt ECSA. The retention of ECSA after 1000 CVs at 80 °C as compared to 5 CVs at that temperature is given in the last column of Table 2.The ECSA values were not transformed into SSA this time, as we do not know how much Pt might have been dissolved. The loss in ECSA tends to be higher for the catalysts having lower initial particle sizes, irrespective of the alloying element or its content. Of the catalysts annealed at 950 °C the loss in ECSA amounted to 20–50%, with PtCo retaining appreciably more surface area than PtNi and PtCu, and indeed Pt. Loss in ECSA could in principle be due to both Pt dissolution and particle growth [29]. The latter is certainly occurring (*vide supra*), but our data are not precise enough to estimate the eventual role played by Pt dissolution.

The specific ORR activities of the aged catalysts calculated at 0.9 V are also presented in Table 3.It is to be noted that the activities at RT and 80 °C cannot be compared in a straightforward manner: the O_2/H_2O standard potential decreases with temperature [42,43], and the oxygen concentration in the electrolyte is lower at 80 °C than at RT, and correcting for this would lead to an increase in the rate constant at 80 °C of a factor of 5–10. But this is not the point here: we only want to compare the specific activities of the alloy catalysts to those of Pt-only ones after ageing at 80 °C, in order to determine whether the alloying effect is still there or not. The respective polarization curves of selected catalysts (PtCo group) are shown in Fig. 9, while that of the other catalysts are given in

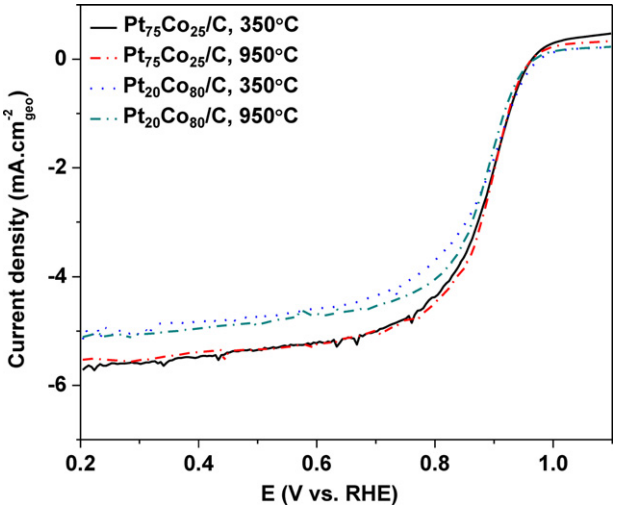

Fig. 9. ORR polarization curves of PtCo/C after 1000 CV scans at 80 °C; conditions: 0.5 M $HClO_4$, 5 mV/s, O_2 atmosphere, 1600 rpm.

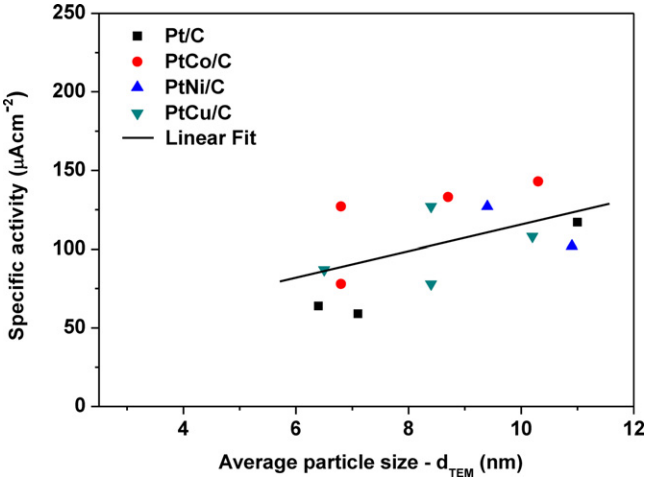

Fig. 10. Specific activity of the catalysts at 0.9 V as the function of particle size (d_{TEM}) after the durability tests at 80 °C: (■) Pt/C, (●) PtCo/C, (▲) PtNi/C and (▼) PtCu/C.

Supplementary Fig. S3. The specific activities are plotted against the particle size, as determined by TEM, in Fig. 10. For Pt/C itself the catalysts annealed at 350 °C and 600 °C still under perform with respect to the 950 °C annealed one. This is more or less in line with the measured average particle sizes (see Table 1). For the alloys the situation is not quite as neat, but taken all together one can conclude that $Pt_{75}Co_{25}$/C along with the non-noble metal-rich alloys show specific activities slightly higher (about 1.2 times) to that of 950 °C annealed Pt, but the specific activities of the other alloys are slightly below that of Pt. In other words, any advantage that any alloy catalysts may have had initially has largely disappeared after ageing at 80 °C under the conditions applied here. As the amount of Pt dissolved into the electrolyte during voltage cycling is not studied, the mass activity of the catalysts could not be determined.

The main upshot of the present study is that a thousand potential cycles (0.6–1.2 V) at 80 °C is sufficient to reduce the specific ORR activity of PtM (M = Co, Ni, Cu) alloys to that of Pt itself. This appears to be due to two main factors: (i) durability testing leads to an increase of particle size beyond the range in which a strong particle-size effect on the ORR activity occurs, and (ii) the non-noble metal component is almost completely leached out. To be sure, 5–10 at% of it is still left in the aged electrodes (EDS), but XPS study of three representative PtCo, PtNi, and PtCu catalysts shows (Fig. 11) that the M component cannot be detected with this technique, implying that the small amount that remains is deeply buried inside relatively massive particles, thus accounting for the equivalent to Pt/C ORR activity. In this respect, the results obtained with PtM electrodeposits [35] form an interesting contrast. Although the initial particle size, as determined with TEM, is rather similar to that of the PtM/C catalysts, alloy electrodeposits retain appreciably more non-noble metal, which, moreover, remains detectable with XPS, showing that it is sitting in subsurface positions, and, hence, the alloys retain an activity advantage over Pt. On the origin of this state of affairs we can only speculate. It is noted in this connection that Pt alloy stability at 80 °C vis-à-vis Pt itself has also been differently evaluated in the literature: Wakabayashi et al. [39] report that for sputtered alloys the ORR activity advantage is lost upon testing at temperatures higher than 60 °C where they ascribe this loss to the formation of a thick Pt-skin (as we do for our Pt alloy particles, above), while Neyerlin et al. [32] find that carbon-supported PtCu(Co) alloys retain some of their advantage. However, there are instances where the presence of Au on the surface [40] or in the subsurface layers [41] suppress the dissolution of surface Pt and hence keeps the particle morphology intact. These types of catalysts (Pt and Pt alloys) with

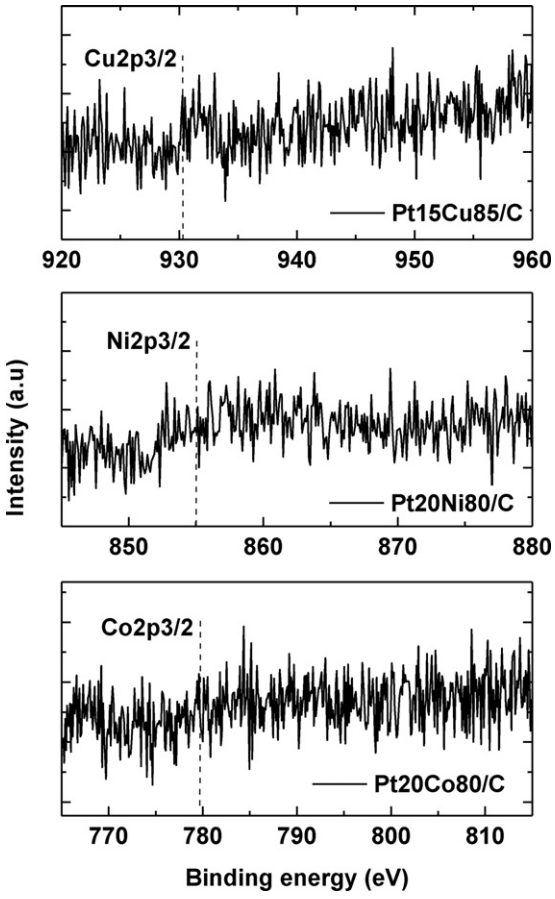

Fig. 11. X-ray photoelectron spectra showing the Co, Ni and Cu 2p regions from the surface of Pt alloys after 1000 CV scans at 80 °C.

controlled morphology and composition profile are found to have superior durability than the regular Pt/C and PtM/C catalysts.

Unlike fresh catalysts, the hydrogen adsorption/desorption regions of the CVs after the durability tests at 80 °C become quite similar. This shows that the particle morphology (geometric factor) of the catalysts becomes fairly similar after undergoing various processes such as non-noble metal dissolution, surface Pt reconstruction and particle growth.

In general, as mentioned in Section 1, one could expect to find that the specific activity of Pt alloys would depend on the particle size, and on the amount and type of alloying element. And preferably, this dependency should be also traceable in the cyclic voltammetry, *e.g.* in the Pt oxide reduction peak potential, or the structure of the H_{upd} region, since even if strain in the Pt surface layer is the driving force behind increased ORR performance, this should manifest itself in other reactivity parameters as well. Our data on the CV and ORR activity of stabilized catalysts (25 CVs) at room temperature, do indicate that both these things change with the particle size, and vary with alloying element, but only rough trends could be identified: small particles have (as expected) a lower specific ORR activity than large ones, and PtCu and PtCo appear to outperform the PtNi alloys and Pt itself. More precise relationships have proved elusive. After the durability tests, the specific activity of the catalysts becomes quite similar and show only a weak dependence on the particle size.

4. Conclusions

Well-defined carbon-supported Pt and PtM alloys with M = Co, Ni and Cu were made in a similar way (synthesis, annealing) to

compare their activity and durability for the oxygen reduction reaction as a function of the alloying element in a systematic manner. Pt-rich PtCo/C and PtCu/C alloys were formed by annealing at 350 °C, whereas annealing at 950 °C was required to obtain Co- or Cu-rich alloys. Single-phase PtNi/C alloys were only formed by a high temperature-annealing step.

Non-noble metal rich alloys and $Pt_{75}Cu_{25}$/C reduced at 950 °C were perceived to have the highest activity after the initial stabilization process of 25 CV scans at room temperature. Even though the particle size of Pt/C and non-noble metal-rich alloys formed at 950 °C are similar, non-noble metal-rich alloys exhibited about 2–3 times higher specific activity than Pt. However, for the catalysts reduced at 350 °C and with similar particle size range no gain in the specific activity was obtained for the alloys over Pt(except $Pt_{75}Co_{25}$/C). As a group, the performance of PtCo and PtCu alloys was found to be most attractive when compared to PtNi alloys and Pt. Like Pt, specific activity of Pt alloys was found to depend on the particle size: the lower the particle size the lower the specific activity.

Durability tests at 80 °C by voltage cycling led to substantial deactivation of the alloy catalysts vis-à-vis Pt. The specific activity of the aged catalysts annealed at a similar temperature is quite comparable. The alloying effect is almost completely lost due to dissolution of about 90–95 at% non-noble metals with the surface only consisting of Pt after the durability tests, and only a weak particle-size effect remains.

Acknowledgements

This work was part of the Dutch EOSLT Consortium PEMFC, Contract nos. EOSLT 06005 and EOSLT 07005, supported by the Ministry of Economic Affairs.

Appendix A. Supplementary data

Supplementary data associated with this article can be found, in the online version, at doi:10.1016/j.apcatb.2011.11.003.

References

[1] F.A. de Bruijn, V.A.T. Dam, G.J.M. Janssen, Fuel Cells 8 (2008) 3.
[2] W. Vielstich, A. Lamm, H. A. Gasteiger, Handbook of Fuel Cells, Fundamentals Technology and Applications, 2003.
[3] R. Borup, J. Meyers, B. Pivovar, Y.S. Kim, R. Mukundan, N. Garland, D. Myers, M. Wilson, F. Garzon, D. Wood, P. Zelenay, K. More, K. Stroh, T. Zawodzinski, J. Boncella, J.E. McGrath, M. Inaba, K. Miyatake, M. Hori, K. Ota, Z. Ogumi, S. Miyata, A. Nishikata, Z. Siroma, Y. Uchimoto, K. Yasuda, K.I. Kimijima, N. Iwashita, Chem. Rev. 107 (2007) 3904.
[4] V.A.T. Dam, K. Jayasayee, F.A. de Bruijn, Fuel Cells 9 (2009) 453.
[5] H.A. Gasteiger, S.S. Kocha, B. Sompalli, F.T. Wagner, Appl. Catal. B 56 (2005) 9.
[6] W. Schmittinger, A. Vahidi, J. Power Sources 180 (2008) 1.
[7] Y.Y. Shao, G.P. Yin, Y.Z. Gao, J. Power Sources 171 (2007) 558.
[8] S.S. Zhang, X.Z. Yuan, J.N.C. Hin, H.J. Wang, K.A. Friedrich, M. Schulze, J. Power Sources 194 (2009) 588.
[9] S.C. Ball, S.L. Hudson, D. Thompsett, B. Theobald, J. Power Sources 171 (2007) 18.
[10] J. Zhang, M.B. Vukmirovic, K. Sasaki, A.U. Nilekar, M. Mavrikakis, R.R. Adzic, J. Am. Chem. Soc. 127 (2005) 12480.
[11] S. Koh, P. Strasser, J. Am. Chem. Soc. 129 (2007) 12624.
[12] S. Mukerjee, S. Srinivasan, J. Electroanal. Chem. 357 (1993) 201.
[13] U.A. Paulus, A. Wokaun, G.G. Scherer, T.J. Schmidt, V. Stamenkovic, V. Radmilovic, N.M. Markovic, P.N. Ross, J. Phys. Chem. B 106 (2002) 4181.
[14] T. Toda, H. Igarashi, H. Uchida, M. Watanabe, J. Electrochem. Soc. 146 (1999) 3750.
[15] V. Stamenkovic, T.J. Schmidt, P.N. Ross, N.M. Markovic, J. Phys. Chem. B 106 (2002) 11970.
[16] V. Stamenkovic, T.J. Schmidt, P.N. Ross, N.M. Markovic, J. Electroanal. Chem. 554 (2003) 191.
[17] V.R. Stamenkovic, B.S. Mun, M. Arenz, K.J.J. Mayrhofer, C.A. Lucas, G.F. Wang, P.N. Ross, N.M. Markovic, Nat. Mater. 6 (2007) 241.
[18] I. Dutta, M.K. Carpenter, M.P. Balogh, J.M. Ziegelbauer, T.E. Moylan, M.H. Atwan, N.P. Irish, J. Phys. Chem. C 114 (2010) 16309.
[19] P. Mani, R. Srivastava, P. Strasser, J. Phys. Chem. C 112 (2008) 2770.
[20] P. Mani, R. Srivastava, P. Strasser, J. Power Sources 196 (2011) 666.
[21] P. Strasser, Adv. Mater. Proc. 166 (2008) 13.
[22] P. Strasser, Rev. Chem. Eng. 25 (2009) 255.
[23] P. Strasser, S. Koh, T. Anniyev, J. Greeley, K. More, C.F. Yu, Z.C. Liu, S. Kaya, D. Nordlund, H. Ogasawara, M.F. Toney, A. Nilsson, Nat. Chem. 2 (2010) 454.
[24] V. Stamenkovic, B.S. Mun, K.J.J. Mayrhofer, P.N. Ross, N.M. Markovic, J. Rossmeisl, J. Greeley, J.K. Norskov, Angew. Chem. -Int. Ed. 45 (2006) 2897.
[25] A. Bonakdarpour, J. Wenzel, D.A. Stevens, S. Sheng, T.L. Monchesky, R. Lobel, R.T. Atanasoski, A.K. Schmoeckel, G.D. Vernstrom, M.K. Debe, J.R. Dahn, J. Electrochem. Soc. 152 (2005) A61.
[26] K. Jayasayee, V.A. Dam, T. Verhoeven, S. Celebi, F.A. de Bruijn, J. Phys. Chem. C 113 (2009) 20371.
[27] S. Chen, W.C. Sheng, N. Yabuuchi, P.J. Ferreira, L.F. Allard, Y. Shao-Horn, J. Phys. Chem. C 113 (2009) 1109.
[28] S. Chen, P.J. Ferreira, W.C. Sheng, N. Yabuuchi, L.F. Allard, Y. Shao-Horn, J. Am. Chem. Soc. 130 (2008) 13818.
[29] S. Chen, H.A. Gasteiger, K. Hayakawa, T. Tada, Y. Shao-Horn, J. Electrochem. Soc. 157 (2010) A82.
[30] H.R. Colon-Mercado, B.N. Popov, J. Power Sources 155 (2006) 253.
[31] P. Yu, M. Pemberton, P. Plasse, J. Power Sources 144 (2005) 11.
[32] K.C. Neyerlin, R. Srivastava, C.F. Yu, P. Strasser, J. Power Sources 186 (2009) 261.
[33] N.M. Markovic, P.N. Ross, Surf. Sci. Rep. 45 (2002) 121.
[34] C. Wang, D. van der Vliet, K.C. Chang, H.D. You, D. Strmcnik, J.A. Schlueter, N.M. Markovic, V.R. Stamenkovic, J. Phys. Chem. C 113 (2009) 19365.
[35] K. Jayasayee, Durability of Cathode Catalyst Components of PEM Fuel Cells, PhD Thesis, Eindhoven University of Technology, 2011.
[36] N. Markovic, H. Gasteiger, P.N. Ross, J. Electrochem. Soc. 144 (1997) 1591.
[37] B.C. Beard, P.N. Ross, J. Electrochem. Soc. 137 (1990) 3368.
[38] K.H. Kangasniemi, D.A. Condit, T.D. Jarvi, J. Electrochem. Soc. 151 (2004) E125.
[39] N. Wakabayashi, M. Takeichi, H. Uchida, M. Watanabe, J. Phys. Chem. B 109 (2005) 5836.
[40] J. Zhang, K. Sasaki, E. Sutter, R.R. Adzic, Science 315 (2007) 220.
[41] C. Wang, D. Van der Vliet, K.L. More, N.J. Zaluzec, S. Peng, S. Sun, H. Daimon, G. Wang, J. Greeley, J. Pearson, A.P. Paulikas, G. Karapetrov, D. Strmcnik, N.M. Markovic, V.J. Stamenkovic, Nano Lett. 11 (2011) 919.
[42] C. Song, J. Zhang, Chapter 2, PEM Fuel Cell Electrocatalysts and Catalysts Layers, Fundamentals and Applications, 2008.
[43] C. Song, Y. Tang, J.L. Zhang, J. Zhang, H. Wang, J. Shen, S. McDermid, J. Li, P. Kozak, Electrochim. Acta 52 (2011) 2552.